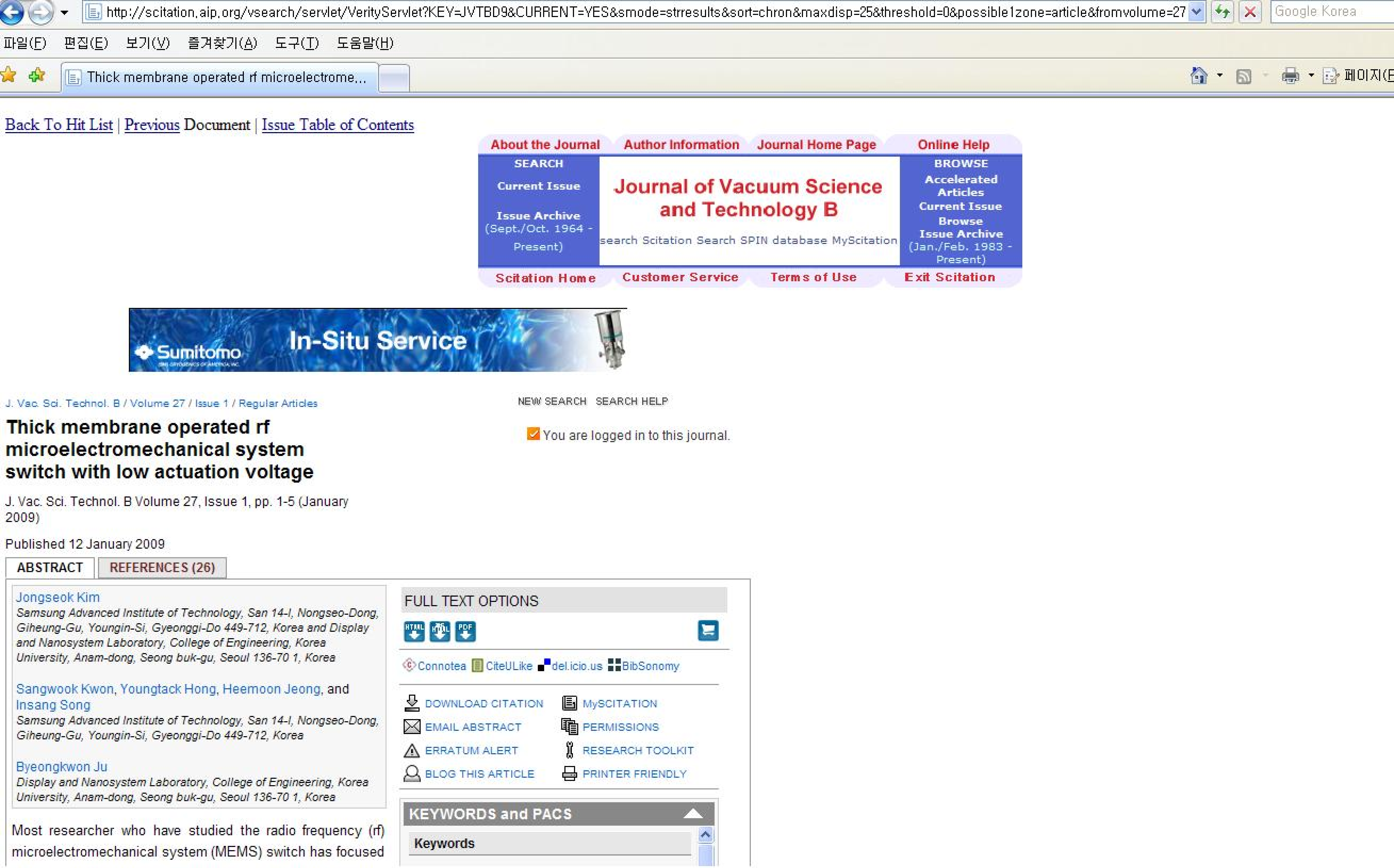

Journal of Vacuum Science and Technology B

J. Vac. Sci. Technol. B / Volume 27 / Issue 1 / Regular Articles

Thick membrane operated rf microelectromechanical system switch with low actuation voltage

J. Vac. Sci. Technol. B Volume 27, Issue 1, pp. 1-5 (January 2009)

Published 12 January 2009

Jongseok Kim
Samsung Advanced Institute of Technology, San 14-l, Nongseo-Dong, Giheung-Gu, Youngin-Si, Gyeonggi-Do 449-712, Korea and Display and Nanosystem Laboratory, College of Engineering, Korea University, Anam-dong, Seong buk-gu, Seoul 136-70 1, Korea

Sangwook Kwon, Youngtack Hong, Heemoon Jeong, and Insang Song
Samsung Advanced Institute of Technology, San 14-l, Nongseo-Dong, Giheung-Gu, Youngin-Si, Gyeonggi-Do 449-712, Korea

Byeongkwon Ju
Display and Nanosystem Laboratory, College of Engineering, Korea University, Anam-dong, Seong buk-gu, Seoul 136-70 1, Korea

Most researcher who have studied the radio frequency (rf) microelectromechanical system (MEMS) switch has focused

Thick membrane operated rf microelectromechanical system switch with low actuation voltage

Jongseok Kim
Samsung Advanced Institute of Technology, San 14-I, Nongseo-Dong, Giheung-Gu, Youngin-Si, Gyeonggi-Do 449-712, Korea and Display and Nanosystem Laboratory, College of Engineering, Korea University, Anam-dong, Seong buk-gu, Seoul 136-70 1, Korea

Sangwook Kwon, Youngtack Hong, Heemoon Jeong, and Insang Song
Samsung Advanced Institute of Technology, San 14-I, Nongseo-Dong, Giheung-Gu, Youngin-Si, Gyeonggi-Do 449-712, Korea

Byeongkwon Ju[a)]
Display and Nanosystem Laboratory, College of Engineering, Korea University, Anam-dong, Seong buk-gu, Seoul 136-70 1, Korea

(Received 2 July 2008; accepted 27 October 2008; published 12 January 2009)

Most researcher who have studied the radio frequency (rf) microelectromechanical system (MEMS) switch has focused on the electrostatic actuation types switch because of this type's low power consumption, simple fabrication method, and good rf characteristics compared to magnetic, thermal, and piezoelectric driving method. However, most of electrostatic actuation type switch needs high operation voltage compared to other types. One of the reasons that affect the high operation voltage is the bending of the membrane because of an internal stress gradient. This bending increases the gap between electrode and membrane. To solve this problem, the authors developed the thick membrane operated seesaw type rf MEMS switch. This membrane consisted of a pivot under single crystal thick silicon membrane for a seesaw mode operation and a flexible spring for an up-down actuation mode. After the fabrication of this switch, the authors measured its rf characteristics. The minimum actuation voltage was about 12 V, the isolation is about −50 dB, and the insertion loss was about −0.2 dB at 2 GHz, respectively. © *2009 American Vacuum Society.*
[DOI: 10.1116/1.3032916]

I. INTRODUCTION

rf microelectromechanical system (MEMS) devices have been proven to be one of the valuable technologies for high performance components and systems applications.[1–4] Among these devices, micromechanical rf switches offer many benefits such as low insertion loss, good isolation, the excellent linearity characteristics, and low power consumption compared to conventional semiconductor switch.[5–12] This technology have made possible the design and fabrication of control devices suitable for switching microwave signals. As a consequence, these micromechanical switch development companies and institutes were continuously trying to replace the *p*-*i*-*n* diode or junction field effect transistor base semiconductor switches with micromechanical switches in wireless communication devices, such as multiband selectors and filter banks.[13,14] Various types of switch, including low voltage based carbon nanotube mechanical rf switch, have been developed in the past decade and recently.[15,16] Among these switches, the conventional seesaw type switch has several merits such as a good isolation and a membrane antistiction. However, to obtain the required restoring force and contact force, voltage was needed to increase.[17] The conventional membrane type switches also have several advantages such as a low power consumption, a simple fabrication method, and good rf characteristics. However, these switches also needed a high driving voltage of 20–50 V to ensure the restoring force of the membrane.[18–22] In these type of switches, the driving voltage was very critical to the gap between the electrode and membrane.[23] The residual stress during fabrication processes often resulted in locally different bending of the membrane that caused gap change between electrode and membrane. This change originated the increase in driving voltage and its variation. To prevent this membrane bending problem, we proposed a thick membrane seesaw type rf MEMS switch. This membrane was made of a single crystalline bulk silicon to reduce the bending. However, this thick membrane needed a high actuation voltage because of high restoring force of the membrane. To solve these problems, we introduced a flexible spring for low action voltage and pivot under the membrane for high restoring force. When the membrane was actuated downward, it operated in a seesawlike mode. This new concept made up for the high voltage characteristic of the conventional seesaw mode actuated switch that was required for obtaining the necessary restoring force and contact force. We also obtained a voltage decrease comparable to the membrane type switch while maintaining high isolation comparable to the seesaw type switch.

[a)] Tel.: +82-2–3290-3671; electronic mail: bkju@korea.ac.kr

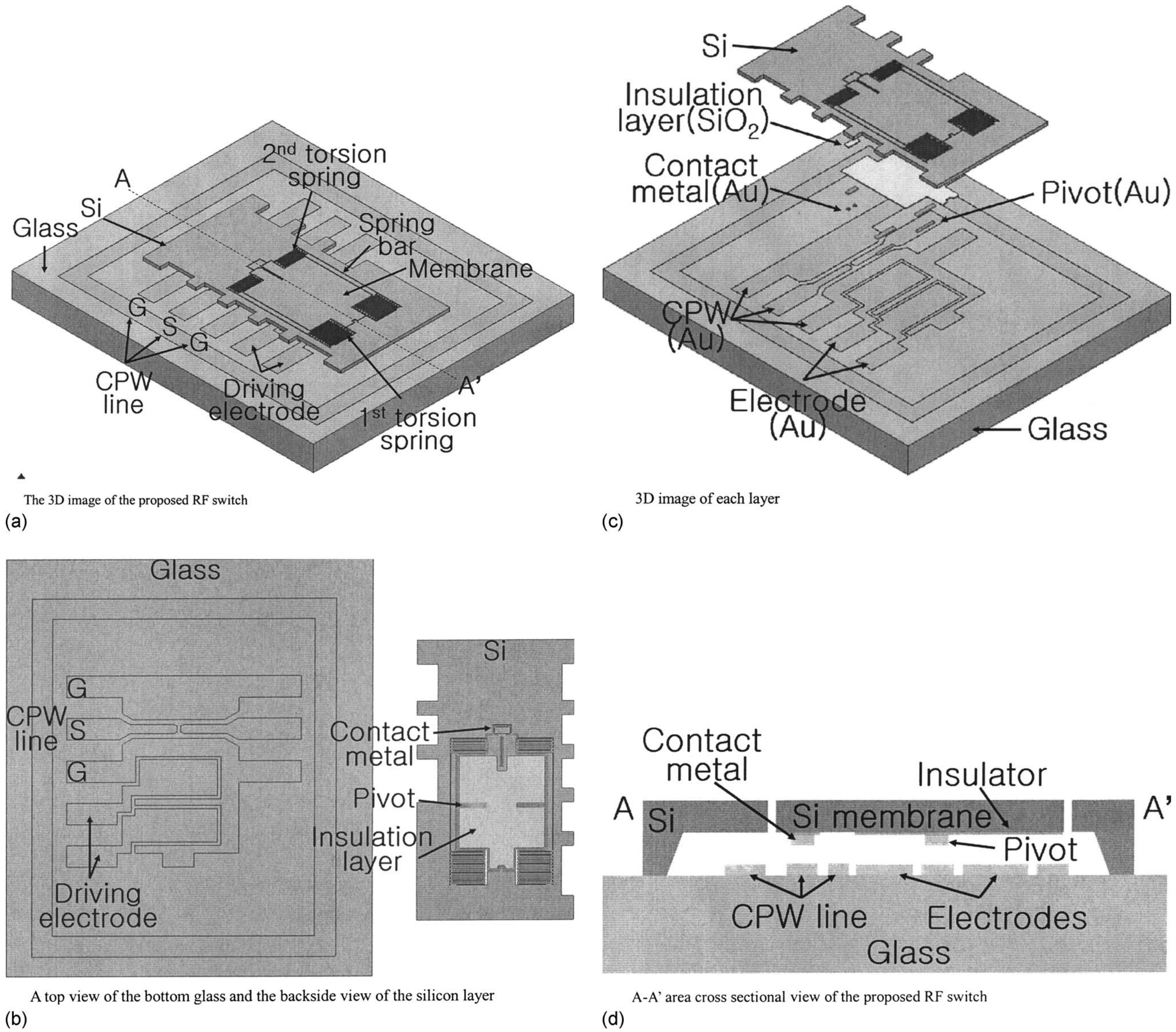

The 3D image of the proposed RF switch
(a)

3D image of each layer
(c)

A top view of the bottom glass and the backside view of the silicon layer
(b)

A-A' area cross sectional view of the proposed RF switch
(d)

FIG. 1. Schematic of the proposed rf switch. (a) The 3D image of the proposed rf switch. (b) A top view of the bottom electrode and the back side view of the membrane. (c) 3D image of each layer. (d) *A-A'* area cross sectional view of the proposed rf switch.

II. DESIGN AND SIMULATION

A three-dimensional (3D) and plane detail image of our concept design were shown in Fig. 1. Our switch was made of bonded glass and silicon wafer. On the glass wafer, a coplanar wave guide (CPW) line and electrode pad were designed and patterned for the rf signal pass and membrane operation. The thick membrane with pivot and folded springs for membrane actuation were formed on the silicon wafer. This repeated folded spring decreased the actuation voltage due to the low spring constant and this spring constant decreased linearly with the successive addition of the folded spring.[24] The end of the first folded spring was connected to the anchored silicon which was bonded with glass, and the end of the second folded spring was connected to the membrane. The spring bar coupled the first and second springs. Figure 2 showed the simplified operating mode of the proposed rf switch. While driving voltage was not applied to the electrodes, the switch was in the "off" state. dc driving voltage was applied to the contact electrode, the membrane was actuated downward and the contact pad metal connected the broken CPW line. At this time, the switching state changed to the "on" state, the electrode and membrane had a 1 μm gap. This very narrow gap was maintained without bending or stiction because of the 30 μm thickness membrane and pivot. This narrow gap also made it possible to operate the switch at a very low voltage. When the dc voltage was applied to the restoring electrode, contact pad metal was elaborated and separated from broken signal line. From this time, this membrane operated like a seesaw and the switching state changed to the off state. As long as the dc voltage was applied to the driving electrode or restoring electrode, this seesaw mode operation was repeated.

Total size of the designed switch was 1.2×1.5 mm^2. The width of the CPW signal line on the glass wafer was 50 μm

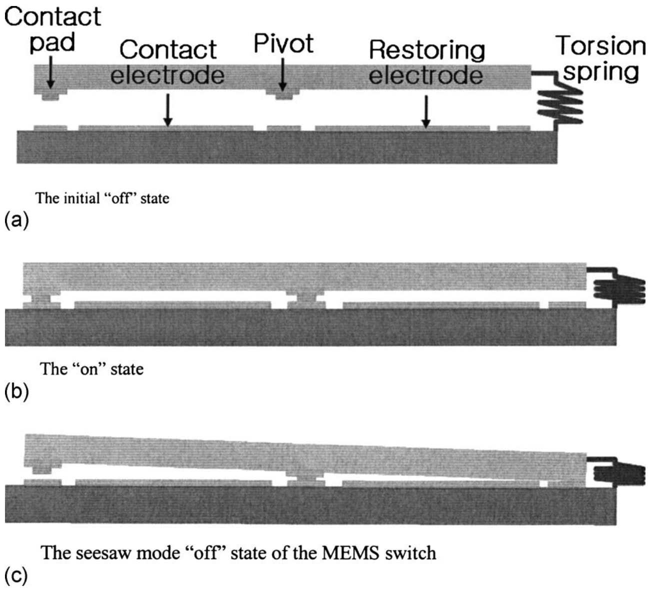

FIG. 2. Simplified operating mode of the proposed rf MEMS switch. (a) The initial off state. (b) The on state. (c) The seesaw mode off state of the MEMS switch.

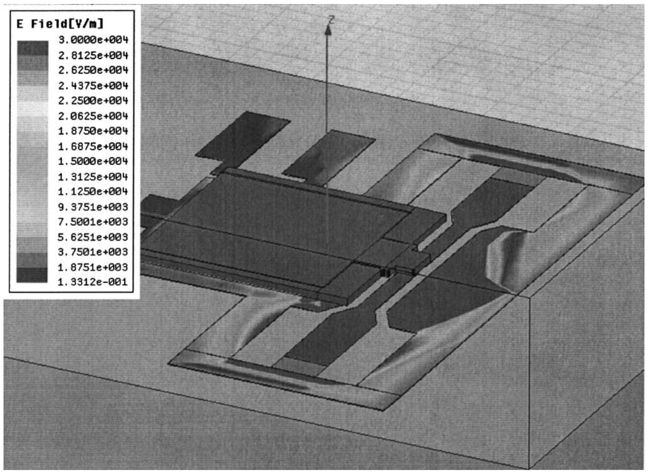

FIG. 3. rf simulated results of the purposed switch.

and the initial gap between the signal and ground line was 3 μm. The gap of broken CPW signal lines was 20 μm. The length of folded spring line was 190 μm and its width was 5 μm. The first folded spring consisted of four meander springs; the second folded spring consisted of ten meander springs. A pivot was formed under the center of the membrane and the size of each of the pivots was $150\times 20\ \mu\text{m}^2$. This pivot was used for the seesaw mode operation when the membrane was actuated downward. To estimate the rf characteristic of our design, high frequency structural simulator was used. Figure 3 showed the simulated results of our design. Simulated insertion loss of our design is −0.15 dB and isolation was −41.4 dB at 2 GHz.

III. EXPERIMENT AND FABRICATION

Figure 4 showed the fabrication process flow of purposed rf switch. 500 μm thickness "Corning 7740 Pyrex" glass wafer was used as a substrate wafer to minimize the coefficient of thermal expansion mismatch problem.[25] To form the CPW line and electrode, Cr/Au 50/1000 nm was sputtered on the wafer and defined by using an wet etching process. The membrane with the spring and pivot was formed on a silicon wafer, and detailed fabrication process was described as follows. The silicon wafer was a p-type, (100) with a resistivity of 0.01–0.02 Ω cm. 500 nm thickness thermal oxide layer was deposited on the silicon wafer using wet oxidation method. Oxide layer was pattern using photoresist and reactive ion etcher (RIE) to form the silicon cavity etch mask pattern. Exposure silicon layer was etched using tetramethylammonium hydroxide 20% wet. solution. The temperature of during ech process was 90 °C, etch rate was about 0.8 μm/min, and 4.5 μm depth was etched. After etching process, thermal oxide layer was stripped using HF solution. To form an insulation layer, 500 nm of oxide was deposited on the cavity using plasma enhanced chemical vapor deposition and patterned using RIE. On the insulation layer, Au layer was deposited and patterned by a wet etching method to fabricate the contact metal. During the photolithography of the insulation layer and contact metal layer, 4.5 μm gap existed between mask and photoresister. However, the $80\times 30\ \mu\text{m}^2$ size oxide insulation and the $70\times 20\ \mu\text{m}^2$ size contact metal layer was clearly patterned without distortion. After the completion of the fabrication process of the each wafer, we added the initial cleaning process just before the bonding of two wafers. Surface cleaning was very important because minor contamination of the glass or Si surface seriously deteriorated bonding performance or strength.[26] We used $H_2SO_4:H_2O_2=1:1$ solution and the HF dipping method for cleaning the surface of the wafers: 1 min dipped in the $H_2SO_4:H_2O_2=1:1$ solution and 10 s dipped in the HF solution. After the dipping in the solutions, we aligned the glass and silicon wafer through the back side of the glass substrate and anodic bonding method was used. The bonding temperature was 380 °C and the pressure was 100 N. A 600 V dc voltage was applied for 5 min. The advantages of this separate process were not only effective for avoiding the contamination which could be from the sacrificial layer residue and for securing the reliability of the contact metal, but the process was also effective for precision gap control determined by the metal thickness or cavity depth. After the bonding of two wafers, silicon layer was polished until 30 μm remained. Silicon structure must be connected with ground metal pad. So, Si layer on the ground pad was patterned and etched using an inductively coupled plasma RIE (ICP-RIE). Au/Cr 1 μm/50 nm was deposited using sputter and patterned using wet etch method to connect the silicon and ground metal pad. The membrane structure was patterned on the polished Si layer and etched by using an ICP-RIE. The structure patterned photoresist was removed by using a dry asher. In order to prevent the thermal stress and the bending of membrane or spring, a low temperature asher was used. Table I indicated the fabrication main parameters of the purposed switch.

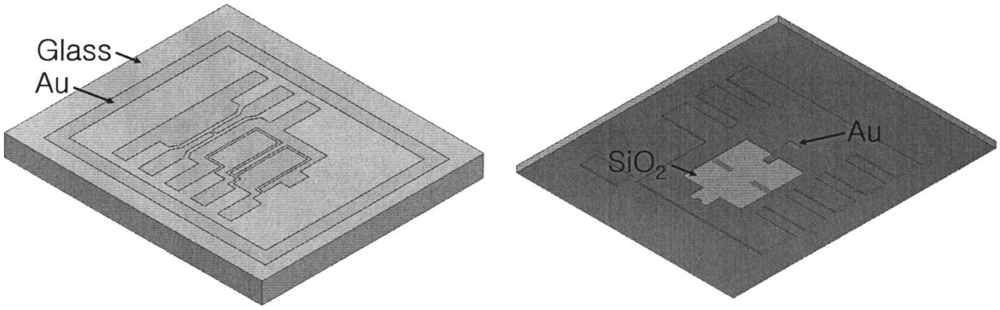

Signal line and electrodes formation

(a)

Pivot and contact pad formation

(d)

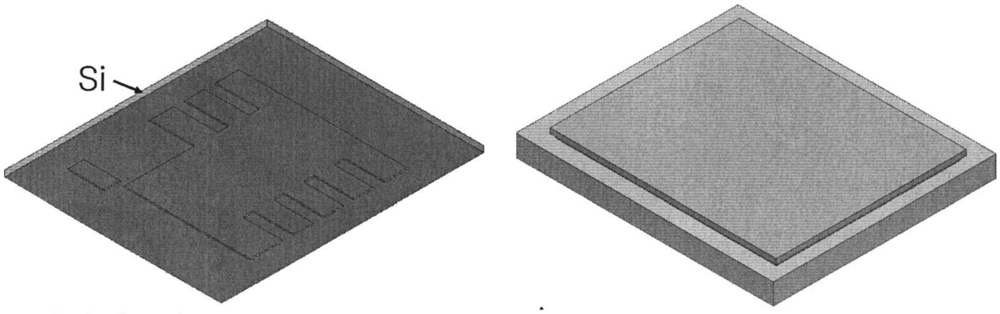

Cavity formation

(b)

Glass and silicon wafer bonding

(e)

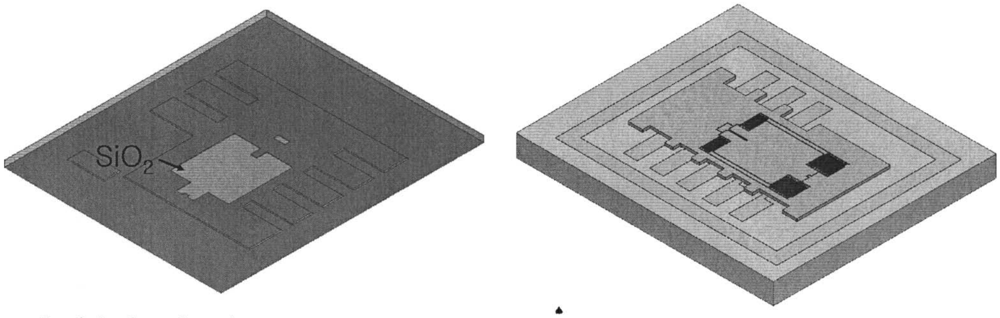

Insulation layer formation

(c)

Membrane formation

(f)

FIG. 4. Fabrication process for the proposed MEMS switch. (a) Signal line and electrodes formation. (b) Cavity formation. (c)Insulation layer formation. (d) Pivot and contact pad formation. (e) Glass and silicon wafer bonding. (f) Membrane formation.

IV. RESULTS AND DISCUSSION

The thick membrane seesaw type low voltage actuated rf switch has been developed and tested. This new concept of switch gathered the strong points of a conventional seesaw type and membrane type switch. A thick membrane and pivot make possible to realize the very small gap between the electrodes and membrane and low operation voltage with a seesaw mode operated design. Sacrificial layer was not used to fabricate the membrane structure, contamination and residue problems during removing of the sacrificial layer was minimized. Figure 5 showed the scanning electron microscopy (SEM) image of the fabricated rf switch. The rf characteristics of the switch was measured using an HP 8510C network analyzer and A G-S-G type picoprobe. Pitch size of this probe tip between ground and signal was 250 μm. Insertion loss and isolation were shown in Fig. 6. Insertion loss of this switch was −0.2 dB, isolation was 50 dB at 2 GHz and the actuation voltage was about 12 V. This switch could be used for applications such as phase shifters and reconfigurable antennas at the high frequency range. It could also be used in the antenna diversity SP2T switches and the switched filter bank for 0.8–20 GHz applications.

TABLE I. Fabrication parameters of the proposed rf switch.

Part	Layer	Materials	Thickness
Si	Insulator	oxide	500 nm
	Contract	Au	500 nm
	Membrane	Si	30 μm
	Cavity	Si	4.5 μm
Glass	CPW	Au	1.5 μm

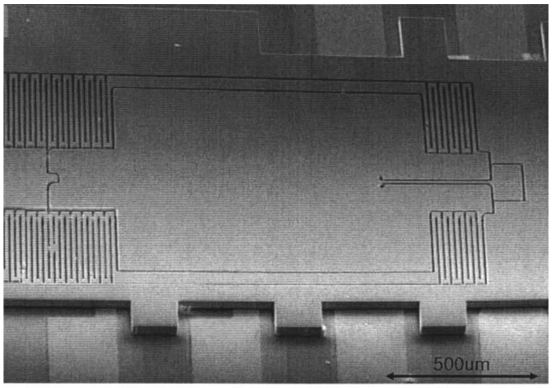

Top side view of fabricated MEMS switch
(a)

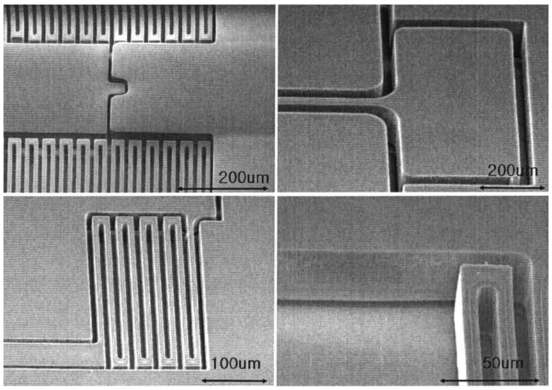

Detail view of MEMS switch
(b)

FIG. 5. SEM image for the fabricated MEMS switch. (a) The side view of fabricated MEMS switch. (b) Detail view of MEMS switch.

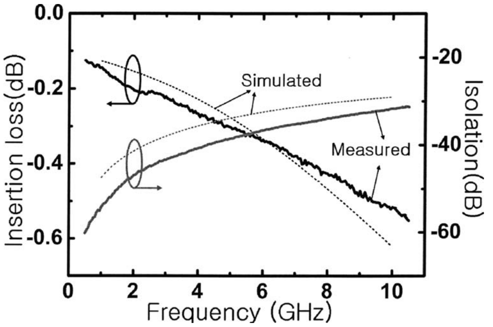

FIG. 6. rf characteristics of the simulated and fabricated rf switch.

ACKNOWLEDGMENTS

This work was supported in part by the National Research Laboratory (NRL), under Contract No. ROA-2007-000-20111-0 Program of the Ministry of Science and Technology Korea Science and Engineering Foundation.

[1] C. L. Goldsmith, A. Malczewski, Z. J. Yao, C. Shea, J. Ehmke, and D. H. Hinzel, Int. J. RF Microwave Comput.-Aided Eng. **9**, 362 (1999).
[2] A. Borgioli, Y. Liu, A. S. Nagra, and R. A. York, IEEE Microw. Guid. Wave Lett. **10**, 7 (2000).
[3] L. P. B. Katehi, J. F. Harvey, and E. Brown, IEEE Trans. Microwave Theory Tech. **50**, 858 (2002).
[4] M. Motiee, R. R. Mansour, and A. Khajepour, J. Vac. Sci. Technol. B **24**, 2499 (2006).
[5] J. N. Randall, C. Goldsmith, D. Denniston, and T. H. Lin, J. Vac. Sci. Technol. B **14**, 3692 (1996).
[6] N. S. Barker and G. M. Rebeiz, IEEE Trans. Microwave Theory Tech. **46**, 1881 (1998).
[7] Z. J. Yao, S. Chen, S. Eshelman, D. Denniston, and C. Goldsmith, J. Microelectromech. Syst. **8**, 129 (1999).
[8] J. B. Muldavin and G. M. Rebeiz, IEEE Trans. Microwave Theory Tech. **48**, 1045 (2000).
[9] S. P. Pacheco, L. P. B. Katehi, and C. T. C. Nguyen, IEEE MTT-S Int. Microwave Symp. Dig. **1**, 165 (2000).
[10] B. A. Cetiner, H. Jafarkhani, Q. Jiang-Yuan, Y. H. Jae, A. Grau, and F. D. Flaviis, IEEE Commun. Mag. **42**, 62 (2004).
[11] W. H. Teh, J. K. Luo, M. R. Graham, A. Pavlov, and C. G. Smith, J. Vac. Sci. Technol. B **21**, 2360 (2003).
[12] T. Morita, K. Nakamatsu, K. Kanda, and Y. Haruyama, J. Vac. Sci. Technol. B **22**, 3137 (2004).
[13] M. Kim, J. B. Hacker, R. E. Mihailovich, and J. F. DeNatale, Angew. Chem., Int. Ed. **11**, 56 (2001).
[14] K. Rangra, B. Margesin, L. Lorenzelli, F. Giacomozzi, C. Collini, M. Zen, G. Soncini, L. del Tin, and R. Gaddi, Sens. Actuators, A **123**, 505 (2005).
[15] A. B. Kaul, E. W. Wong, L. Epp, and B. D. Hunt, Nano Lett. **6**, 942 (2006).
[16] J. Martinez, N. S. Losilla, F. Biscarini, G. Schmidt, T. Borzenko, L. W. Molenkamp, and R. Garcia, Rev. Sci. Instrum. **77**, 086106 (2006).
[17] D. Hah and S. Hong, IEEE Trans. Microwave Theory Tech. **12**, 2540 (2000).
[18] J. J. Yao and M. F. Chang, Proceedings of the Transducers, 1995 (unpublished), p. 384.
[19] C. L. Goldsmith, Z. Yao, S. Eshelman, and D. Denniston, IEEE Microw. Guid. Wave Lett. **8**, 269 (1998).
[20] J. Y. Park, G. H. Kim, K. W. Chung, and J. U. Bu, Sens. Actuators, A **89**, 88 (2001).
[21] S. J. Gross, S. Tadigadapa, T. N. Jackson, S. T. McKinstry, and Q. Q. Zhang, Appl. Phys. Lett. **83**, 174 (2003).
[22] J. J. Hung, L. Dussopt, and G. M. Rebeiz, IEEE Trans. Microwave Theory Tech. **52**, 600 (2004).
[23] G. M. Rebeiz, *RF MEMS: Theory, Design, and Technology* (Wiley, Hoboken, 2003).
[24] J. E. Shigley and L. D. Mitchell, *Mechanical Engineering Design* (McGraw-Hill, New York, 1983).
[25] W. B. Choi, B. K. Ju, Y. H. Lee, M. R. Haskard, M. Y. Sung, and M. H. Oh, J. Vac. Sci. Technol. B **15**, 477 (1997).
[26] G. Wallis and D. I. Pomerantz, J. Appl. Phys. **40**, 3946 (1969).